J Solid State Electrochem (2012) 16:877–882
DOI 10.1007/s10008-011-1435-3

ORIGINAL PAPER

A renewable bamboo carbon/polyaniline composite for a high-performance supercapacitor electrode material

Xinhong zhou · Lanfeng Li · Shanmu Dong · Xiao Chen · Pengxian Han · Hongxia Xu · Jianhua Yao · Chaoqun Shang · Zhihong Liu · Guanglei Cui

Received: 23 March 2011 / Revised: 8 May 2011 / Accepted: 14 May 2011 / Published online: 4 June 2011

Abstract A high-performance conducting polymer-activated carbon composite electrode material was prepared by potentiostatic deposition of aniline on a hierarchically porous carbon, which was carbonized from the natural bamboo. The obtained composite combined the contribution of the unique properties of the activated carbon and pseudocapacitance of the deposited polyaniline layer. This active material possessed excellent rate capability and good cycle performance, over 92% of the original capacitance is retained after 1,000 cycles. The energy density of the composite can reach 47.5 Wh kg^{-1} calculated only by active mass. It can be a good candidate for high-performance supercapacitor.

Keywords Bamboo carbon · Polyaniline · Composite · Supercapacitors · Electrodeposition

Introduction

In recent years, electrochemical supercapacitors as a kind of attractive energy-storage/conversion device are attracting wide interest owing to their higher power density and longer life cycle [1, 2]. Therefore, substantial efforts have been made with regard to the exploration of electrode materials for supercapacitor applications [3–5]. Among various options, activated carbons are commercially available electrode material for supercapacitors because of their high surface area, favorable pore-size distribution, and relatively good electrical conductivity. Activated carbon enjoys a place of pride mainly because of its abundance, cost-effectiveness, and environmentally benign nature [6]. The high surface area and the porosity of the activated carbon are the primary advantages to form an effective double layer, which results in supercapacitive characteristic with a high power density. It is worthwhile to mention that the source of activated carbon from biomass is a natural and renewable one and the preparation process is eco-friendly. Agricultural and food wastes, including banana fiber and coffee bean, have been widely studied in the production of activated carbons [7–13].

Bamboo is taken as a highly utilizable material in many countries because of their fast growth rate, great availability, renewable nature, and short maturity cycle of bamboo culms. The natural bamboo biomass has a fairly constant chemical composition consisting of lignin, cellulose and hemi-cellulose with a well-connected three-dimensional microtexture [14, 15]. After the carbonization of bamboo, the resulting three-dimensional bamboo carbon (BC) with a hierarchical porous structure can provide a large surface area, high conductivity, well-connected, and highly ordered microtexture [16], which facilitate ion transport through providing low-resistance pathways, thus, expecting better performance as supercapacitor electrodes. Polyaniline (PANI) is one of the most promising conducting polymers with high electroactivity, a high doping level and a high specific capacitance, despite suffering from poor life cycle in supercapacitors [17–20]. Herein, bamboo carbon/polyaniline (BC-PANI) composite material by integrating PANI into the electrically conductive framework of BC with higher energy-storage capacity and

X. zhou · L. Li · C. Shang
Qingdao University of Science and Technology,
Qingdao 266101, People's Republic China

S. Dong · X. Chen · P. Han · H. Xu · J. Yao · Z. Liu · G. Cui (✉)
Qingdao Institute of Bioenergy and Bioprocess Technology,
Chinese Academy of Sciences,
Qingdao 266101, People's Republic of China
e-mail: cuigl@qibebt.ac.cn

excellent cycle ability is obtained, which is one of the good candidates for high-performance supercapacitor electrode materials.

Experimental

Preparation of bamboo carbon The natural bamboo was cut into slices, which were then fully impregnated for 4 days at a 1:5 weight ratio of KOH dissolved in a small amount of distilled water and then dried at 100 °C for 12 h. Here, KOH acted as pore-forming agents thereby improving the specific surface area of the material. It was also beneficial to a hydrophilic interface using KOH impregnation step. Activation was then carried out at 900 °C for 5 h under flowing nitrogen at a heating rate of 10 °C min^{-1}. After cooling down to room temperature, the carbonized samples were grinded in a mortar with a pestle, then the received sample was washed in distilled water, filtered, and dried for further evaluation.

Preparation of bamboo carbon/polyaniline composites BC was mixed with 10 wt.% polytetrafluoroethylene (PTFE) binders and cut into plates of 0.5×0.5 cm. The samples were then pasted on a stainless steel current-collector (with the thickness of 150 μm) under a pressure of 15 MPa. The electrodeposition of PANI was carried out in a three-electrode electrochemical cell with the as prepared samples as working electrode, a Pt plate as counter electrode and saturated calomel electrode (SCE) as reference electrode. A typical electrodeposition was performed potentiostatically at 0.75 V (vs SCE) in an aqueous solution of 1 M H_2SO_4 and 0.1 M aniline for different periods (100, 200, 400, and 600 s). The weight of the electrodeposited PANI was estimated by the mass difference of the BC before and after the deposition. The obtained composites were denoted as BC-PANI-100, BC-PANI-200, BC-PANI-400, and BC-PANI-600. After electropolymerization, the BC-PANI composites were washed with distilled water and dried.

Characterization Morphological information was attained from scanning electron microscopy (SEM; HITACHI, S-4800) operated at 10 kV and a transmission electron microscopy (HITACHI H-7650) operated at 200 kV. N_2 adsorption–desorption measurements were carried out at 77 K using a Quantachrome Autosorb gas-sorption system. Brunauer–Emmett–Teller (BET) and Barrett–Joyner–Halenda (BJH) models were used to determine the specific surface areas and the pore sizes of the samples, respectively. Fourier transform infrared (FTIR) spectra were recorded on a NEXUS, Nicolet FTIR spectrometer in the range of 500–4,000 cm^{-1} with KBr pellets.

Electrochemical evaluation A three-electrode cell system was used to evaluate the electrochemical performance by both cyclic voltammetry (CV) and galvanostatic charge–discharge techniques on a CHI 440A instrument (CHI Instrument Inc.) at room temperature. An aqueous solution containing 1 M H_2SO_4 was employed as the electrolyte. The BC and BC-PANI composites were applied as the working electrode, respectively. A Pt plate and a SCE electrode were used as the counter and the reference electrodes, respectively. All the above tests were carried out at ca. 25 °C. The specific gravimetric capacitance was obtained from the discharge process according to the following equation:

$$C_{\mathrm{tot}} = \frac{I\,\Delta t}{m\,\Delta V} \tag{1}$$

Where C_{tot} is the specific gravimetric capacitance (F g^{-1}), I is the current loaded (A), Δt is the discharge time (s), ΔV is the potential change during discharge process, and m is the mass of active material in a single electrode (g).

Results and discussion

The structure of the BC and BC-PANI composite are shown in Fig. 1. From Fig. 1a, we can clearly observe the network structure of BC with fully interconnected macro- and mesoporosity. Such a hierarchical network offers a very good compromise between infiltration rate and surface area. The connecting carbon bridges are nanoporous in themselves (as shown in Fig. 1b). The interconnected macro- and mesopores ensure the electrolyte transport through the material. Microstructures of electrodeposited PANI on BC are presented in Fig. 1c, d, and we can clearly observe the uniform distribution of a porous thin layer of PANI electrodeposited on BC, which is expected to endow a larger supercapacitive contribution.

The BET-specific surface area and porous structure characteristics of the synthesized materials were investigated by nitrogen adsorption–desorption isotherms. The adsorption–desorption isotherm is shown in Fig. 2a, indicating a hysteresis loop characteristic to mesoporous materials. The hysteresis loop in the low relative pressure (P/P_0) range between 0.45 and 0.90 may be ascribed to the presence of a mesoporous structure, and the hysteresis loop P/P_0 between 0.90 and 1.0 might result from the interplates space. According to the BET method, the resulting mesoporous structures present a specific surface area of about 702 m^2 g^{-1}. The pore-size distribution is shown in Fig. 2b, which gives a pore-size distribution of 3.3 nm calculated from the desorption branch of the isotherm using

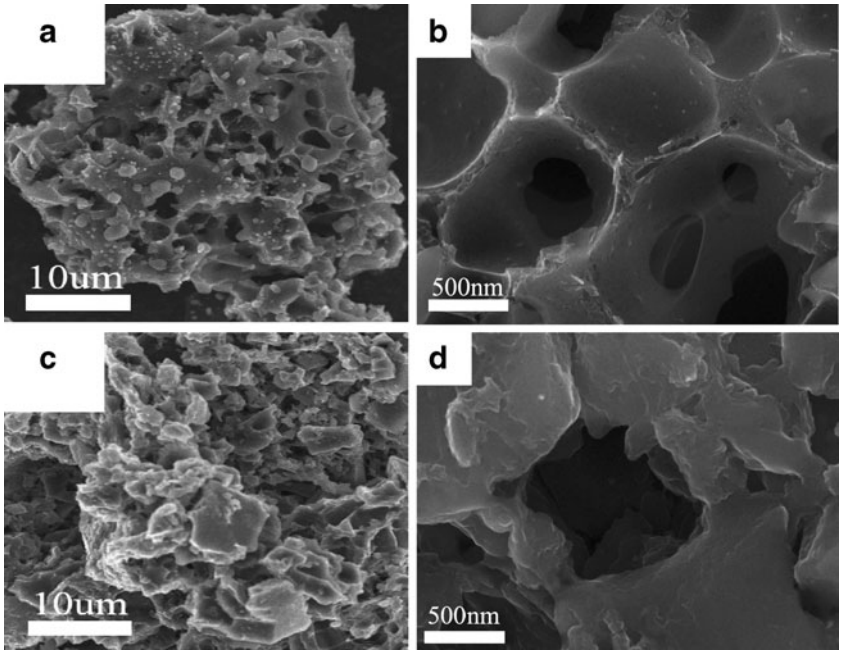

Fig. 1 SEM images of **a**, **b** BC at low and high magnification, respectively; **c**, **d** BC-PANI composite at low and high magnification, respectively

the BJH model. The high BET surface area and excellent mesoporous structure of the BC provides the possibility of efficient transport of electrons and ions, which lead to the high electrochemical capacity of these materials.

The composite structure was proved by FTIR spectroscopy measurement. The FTIR spectra of pure BC, BC-PANI and BC-PTFE-PANI composite are shown in Fig. 3. In the FTIR spectrums, the peaks of pure BC around 2,169, 1,653, and 1,398 cm^{-1} are attributed to carbon dioxide from air, C=O and C–O from the oxygen-containing group in the surface, correspondingly, while the peaks of BC-PTFE centered at 1,212, 1,152, 1,086, and 640–500 cm^{-1} are attributed to the stretching vibration of $–CF_3$ and deformation vibration of C–F. These peaks are all contributed by the PTFE binder. The peaks of PTFE binder is so strong that the weak peaks of pure BC were covered in the FTIR spectrum. Compared with BC-PTFE, several new peaks attributable to PANI appear in the spectrum of BC-PFTE-PANI. A strong and broad peak at 2,902 cm^{-1} indicates the presence of amine and imine units. The origins of the vibrational bands are as follows: 1,560 and 1,432 cm^{-1} bands are assigned to benzenoid ring units; the higher frequency vibration at 1,560 cm^{-1} indicates the stretch vibration of C=N and

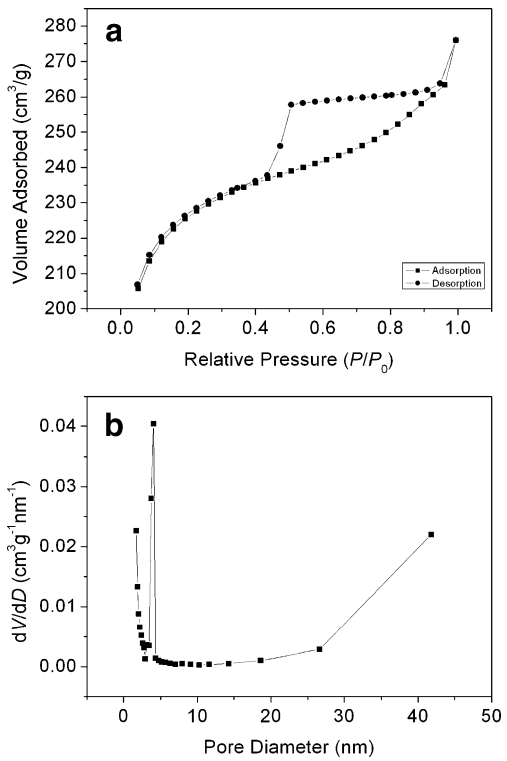

Fig. 2 Nitrogen adsorption–desorption isotherm (**a**) and pore-size distribution (**b**) of the BC material

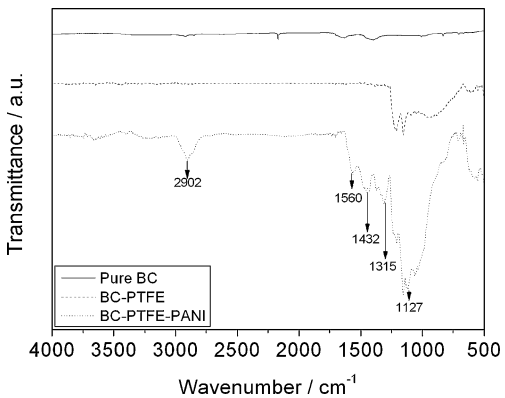

Fig. 3 FTIR spectrum of pure BC, BC-PTFE, and BC-PTFE-PANI composite

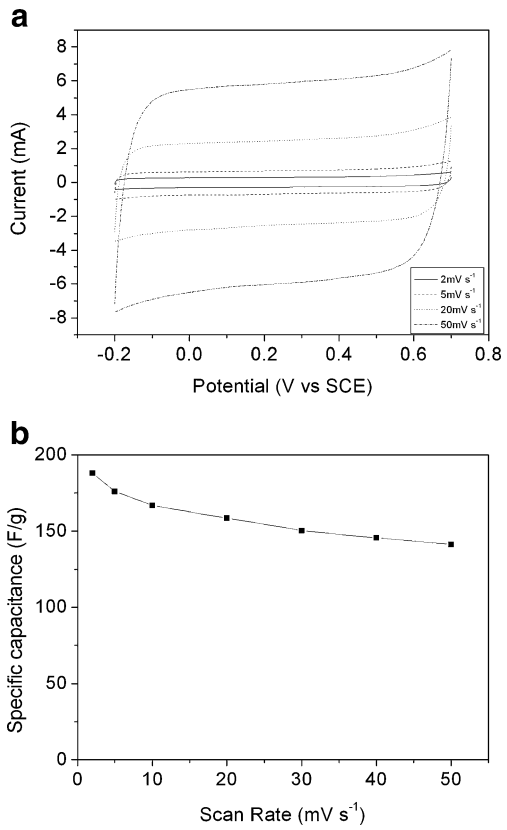

Fig. 4 **a** CV curves of BC in 1 M H_2SO_4 at different scan rates for the first cycle. **b** Specific capacitance of the BC at different scan rates in 1 M H_2SO_4 for the first cycle

C=C of quinondiimine units while the lower frequency mode at 1,432 cm^{-1} contributed from the stretch vibration of the phenylene diamine aromatic ring and C=C, the absorption of aromatic amine (Ar–N) appears at 1,315, and 1,127 cm^{-1} peak is attributable to the vibration of N–Ar–N [21–23]. The result confirmed the successful preparation of the BC-PTFE-PANI composites.

CV curves of BC in 1 M H_2SO_4 at various scan rates are shown in Fig. 4a. With the increasing scan rates from 2 to 50 mV s^{-1}, the CV shapes display comparatively little change and all the CV curves show nearly ideal rectangular shape, indicating the good electrical double-layer capacitive behavior. The steep slope in the current change at the switching potentials indicates a small mass-transfer resistance. Figure 4b shows the specific capacitance (SC) of the BC in 1 M H_2SO_4 at different scan rates. The SC of the BC is estimated by CV. A 188 and 141 Fg^{-1} are achieved for scan rates of 2 and 50 mV s^{-1} which displays good rate retention. The SC of the BC is much higher than the SC value of 60 Fg^{-1} reported by Chan Kim et al., who studied the bamboo-based activated carbons through carbonization and subsequent activation with steam with a specific surface area of about 1,025 m^2 g^{-1}[24]. It could be reasonably ascribed to the activation method and special nanostructure of as-prepared BC in our experiments.

In order to enhance the electrochemical performance, PANI was induced to the BC surface by electrodeposition method with different deposition time. CV and charge–discharge tests were employed to characterize the electrochemical performance of various BC-PANI composites. Figure 5 depicts comparison the CV of a pristine BC with composites BC-PANI-100, BC-PANI-200, BC-PANI-400, and BC-PANI-600 at the scan rate of 5 mV s^{-1}. In contrast to pristine BC with a rectangular shape of CV, the composites display distinct redox peaks. Two pairs of redox peaks can be observed, the first oxidation peak at around 0.2 V is related to the transition of PANI from its semiconducting-state (leucoemeraldine form) to a conducting state (polaronic emeraldine form). The second peak at around 0.45 V is due to the emeraldine–pernigranline transition [18, 25]. The corresponding counter processes can be observed during the reverse scan. For the composite materials, the redox current is found to increase with the amount of coated PANI.

The capacitance performance of the composite materials with different deposition time is shown in Fig. 6. As illustrated in Fig. 6a, the composite electrodes consistently show much higher specific capacitance than that of the pristine BC electrode. The BC-PANI-400 electrode exhibits the highest overall capacitance. The effective utilization of the active species is crucial in the realization of pseudocapacitance. To find out the pseudocapacitive contribution from the PANI, the specific capacitance of pure PANI in the composite was calculated by subtracting the BC capacitance from the overall capacitance of the BC-PANI composite electrode. Figure 6b shows the specific capacitance of PANI in the composite at different deposition time. It can be seen that the specific capacitance of PANI decreases with the increase of the deposition time. The pseudocapacitive contribution from the active material is mainly due to the fast faradic reaction at the electrode surface. When increasing

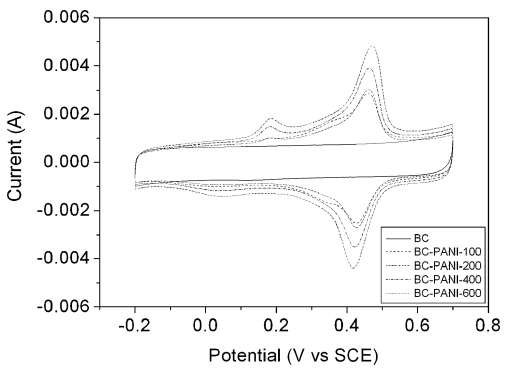

Fig. 5 CV comparison of BC and BC-PANI composites in 1 M H_2SO_4 at the scan rate of 5 mV s^{-1} for the first cycle

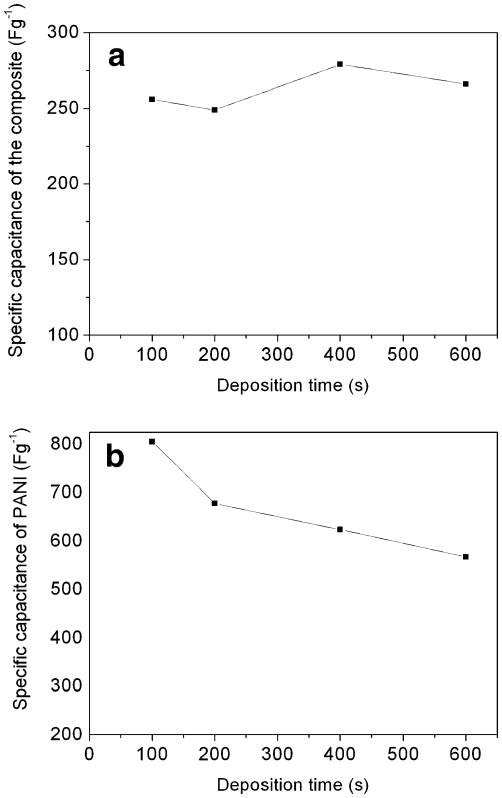

Fig. 6 Specific capacitance of the composite materials (**a**) and specific capacitance of PANI in the composite (**b**) at different deposition time under a scan rate of 2 mV s^{-1} in 1 M H_2SO_4 for the first cycle

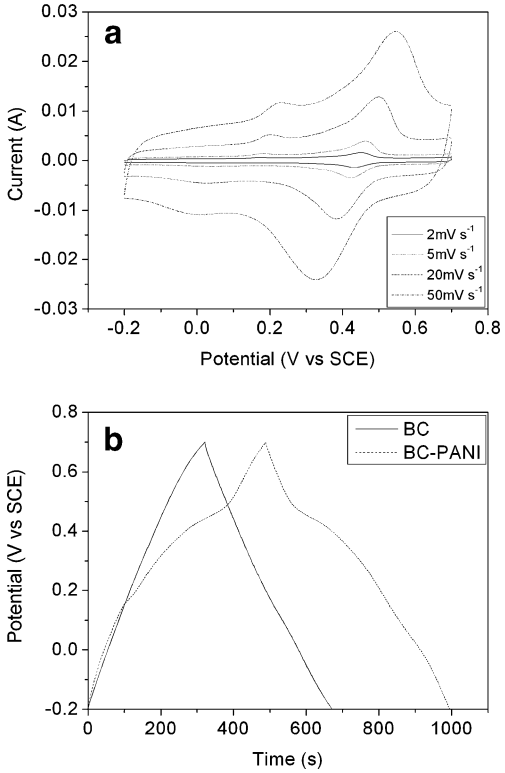

Fig. 7 **a** CV plots at different scan rate for BC-PANI-400 composite in 1 M H_2SO_4 for the first cycle. **b** Charge–discharge performance of BC and BC-PANI-400 composite in 1 M H_2SO_4 at current density of 0.5 A g^{-1} for the first cycle

the deposition time, more and more PANI on the surface of BC was formed. However, the thick PANI layer was not favorable for ion transport and conversely provided a longer transportation pathway. Hence, a thin and porous layer of active material with a short ionic diffusion path is favorable for electrochemical energy storage.

It is observed in Fig. 7a that there is a slight positive shift of the oxidation peaks with an increase in the sweep rates. This is mainly due to a slight increase in the series resistance over porous electrodes at high sweep rates. In addition, as shown in Fig. 7a, the steep slopes at the switching potentials retained after the deposition of PANI at various scan rates, maybe it is because the well-preserved three-dimensionally interconnected porous network with thin layer of PANI on both inner and outer carbon surfaces. The improved capacitance performance after the incorporation of a thin layer of PANI can be clearly seen from the charge–discharge plot shown in Fig. 7b. The electrode potential of bare BC changed linearly with the quantity of electricity passed for the charge and discharge processes. This can be attributed to the charge and discharge of the electrochemical double layer, and is in good agreement with the cyclic voltammetry results showed in Fig. 4a. In contrast, the charge and discharge curves of BC-PANI had a plateau at around 0.45 to 0.50 V vs SCE which indicated a significant redox contribution of PANI. And this is consistent with the cycle voltammetry results shown in Figs. 5 and 7a. At the current density of 0.5 A g^{-1}, the SC was enhanced from 183 F g^{-1} for pristine BC to 277 F g^{-1} for BC-PANI-400 composite. The average SC of BC-PANI-400 composite are calculated to be 277, 266, 244, and 236 F g^{-1} for current densities of 0.5, 1, 2, and 5 A g^{-1}, respectively. Around 85% SC can be retained even when the current density increases by as much as ten times, indicating good rate capability. The energy density

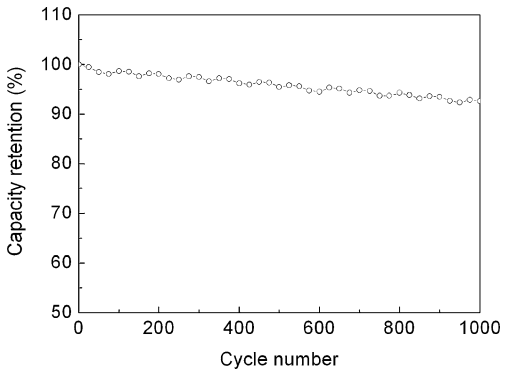

Fig. 8 Cycling performance of BC-PANI-400 composite in 1 M H_2SO_4 under a scan rate of 50 mV s^{-1}

of the composite can reach 47.5 Wh kg^{-1} at a power density of 224 Wkg^{-1}. The SC of BC-PANI-400 composite is much higher than graphene/PANI composite who reported the highest capacitance of 233 Fg^{-1} [26], the rate capability is better than hierarchical nanocomposites of PANI nanowire arrays on graphene oxide sheets and PANI-macroporous carbon composites [27]. The best electrochemical performance was observed on a PANI-porous carbon monolith composite electrode with a specific capacitance of 2,200 Fg^{-1} calculated by the contributed faradic current (not by real weight of PANI) for the pure PANI [28]. The authors also claimed that the electrode performance is largely determined by the structure of the porous carbon monolith, which is consistent with our BC by a facile preparation method. It is reasonably believed that the BC provides a large surface and has a three-dimensionally interconnected porous structure which can greatly shorten the diffusion length, hence providing not only an enhanced energy storage capacity but also a good rate capability.

Figure 8 shows the electrochemical stability of composite electrode BC-PANI-400 under a scan rate of 50 mV s^{-1}. It is seen that over 92% of the original capacitance is retained after 1,000 cycles, indicating a good cycle performance of the composite material. This is mainly because the BC serves as a good support to undertake some mechanical deformation in the redox process of PANI, which avoids destroying the electrode material and is beneficial to a better stability. In addition, this value is better than 46% retention of PANI/CNTs composites reported by Li Fang et al. [29]. The long-term stability implies that the BC-PANI composites are good candidates as a material for supercapacitor electrodes.

Conclusions

A high-performance activated carbon from natural bamboo has been successfully prepared by the simple activation process with a BET-specific surface area of 702 m^2 g^{-1} and an average pore-size distribution of 3.3 nm. It exhibited extraordinary electrochemical performance due to three-dimensionally hierarchical porous structure. The PANI composites have also been well electrodeposited into the BC. The obtained BC-PANI composite combined the essential properties of the carbon substrate and pseudocapacitive behavior of PANI. The electrochemical results showed that the composite electrode possessed excellent capacitive behavior. A 277 and 236 Fg^{-1} are achieved for current densities of 0.5 and 5 Ag^{-1}, which displays good rate capability. Over 92% of the original capacitance is retained after 1,000 cycles, indicating a good cycle performance. It was demonstrated that BC-PANI composite can be a good candidate for high-performance supercapacitor.

Acknowledgments We appreciate the support of "100 Talents" program of the Chinese Academy of Sciences, National Program on Key Basic Research Project of China (973 Program; no. MOST2011CB935700), Shandong Province Fund for Distinguished Young Scientist (BS2009NJ013), and National Natural Science Foundation of China (grant no. 20971077, 20901044, 20802039, and 20902052).

References

1. Conway BE (1999) Electrochemical supercapacitors-scientific fundamentals and technological applications. Plenum, New York
2. Conway BE, Birss V, Wojtowicz J (1997) J Power Sources 66:1
3. Yang G-W, Xu C-L, Li H-L (2008) Chem Commun 48:6537
4. Hu C-C, Chang K-H, Lin M-C, Wu Y-T (2006) Nano Lett 6:2690
5. Sarangapani S, Tilak BV, Chen C-P (1996) J Electrochem Soc 143:3791
6. Frackowiak E, Beguin F (2002) Carbon 40:1775
7. Subramanian V, Luo C, Stephan AM, Nahm KS, Thomas S, Wei B-Q (2007) J Phys Chem C 111:7527–7531
8. Boonamnuayvitaya V, Sae-ung S, Tanthapanichakoon W (2005) Sep Purif Technol 42:159
9. Hwang YJ, Jeong SK, Nahm KS, Shin JS, Stephan AM (2007) J Phys Chem Solids 68:182
10. Nabais JMV, Nunes P, Carrott PJM, Carrott MMLR, Garcia AM, Diaz-Diez MA (2008) Fuel Process Technol 89:262
11. Ahmadpour A, Do DD (1996) Carbon 34:471
12. Lua AC, Yang TJ (2005) Colloid Interface Sci 290:505
13. Ahmadpour A, King BA, Do DD (1998) Ind Eng Chem Res 37:1329
14. Sakata Y, Tanihara YM, Muto A, Uddin MA (1999) Bamboo J 16:41
15. Kurosaki F, Koyanak H, Tsujimoto M, Imamura Y (2008) Carbon 46:850
16. Jiang Q-W, Li G-R, Wang F, Gao X-P (2010) Electrochem Commun 12:924
17. Talbi H, Just PE, Dao LH (2003) J Appl Electrochem 33:465
18. Montilla F, Cotarelo MA, MOrallon E (2009) J Mater Chem 19:305
19. Fusalba F, Gouerec P, Villers D, Belanger D (2001) J Electrochem Soc 148:A1–A6
20. Li D, Huang J-X, Kaner RB (2009) Acc Chem Res 42:135
21. Wan M-X, Li M, Li J-C, Liu Z-X (1994) J Appl Polym 53:131–139
22. Monkman AP, Adams P (1991) Synth Met 40:87–96
23. Sui X-M, Chu Y, Xing S-X (2004) Mater Lett 58:1255–1259
24. Chan K, Lee J-K, Kim J-H, Yang K-S (2006) Korean J Chem Eng 23:592–594
25. Wang Y-G, Li H-Q, Xia Y-Y (2006) Adv Mater 18:2619
26. Xu J-J, Wang K, Zu S-Z, Han B-H, Wei Z-X (2010) ACS Nano 4:5019
27. Wang D-W, Li F, Zhao J-P, Ren W-C (2009) ACS Nano 11:1745
28. Fan L-Z, Hu Y-S, Maier J, Adelhelm P, Smarsly B, Antonietti M (2007) Adv Funct Mater 17:3083
29. Li F, Shi J-J, Qin X (2010) Chinese Sci Bull 11:1100